

Cite this: *Soft Matter*, 2012, **8**, 2875

www.rsc.org/softmatter

PAPER

Injectable thixotropic hydrogel comprising regenerated silk fibroin and hydroxypropylcellulose†

Zuguang Gong,^a Yuhong Yang,^{*b} Qingguang Ren,^b Xin Chen^a and Zhengzhong Shao^{*a}

Received 18th October 2011, Accepted 28th December 2011

DOI: 10.1039/c2sm06984a

In this paper, a novel thixotropic injectable hydrogel has been developed by blending regenerated silk fibroin (SF) and hydroxypropylcellulose (HPC). Dynamic oscillatory rheology showed that the blends gelled at 37 °C within 1 h, and the gelation kinetics and gel properties were controllable by tuning the mix ratio of the blends. The gelation mechanism of such blends was elucidated from morphological observations by confocal laser scanning microscopy (CLSM), structural characterization and a molecular mobility study *via* Raman spectroscopy and quantitative ¹³C-NMR spectroscopy, respectively. The results suggested that the phase separation of the blends triggered the conformational transition of SF from random coil to β -sheet, and thus resulted in the gel network formation through the β -sheet crosslinks and the immobilization of the molecular chain in the dispersed phase. Moreover, it was demonstrated that the blend hydrogel could protect encapsulated cells against high shear force during injection, suggesting that the SF–HPC hydrogel is a promising vehicle for cell delivery. This injectable hydrogel with thixotropic rheological properties was expected to potentially overcome the problem of leakage of liquid precursors to neighboring tissues associated with the *in situ* formation of injectable hydrogels.

1. Introduction

With the intense research efforts in cell transplantation therapy for treatment of various diseases and injuries, there is an increasing need to develop materials for cell delivery, because injecting cells suspended in a liquid medium often results in low cell viability and unsatisfactory functional outcomes.^{1–5} One promising material for such an application is hydrogel.^{6–9} Many efforts have been devoted to implanting cell-encapsulated hydrogels fabricated *ex vivo* into a body site such as bone and cartilage defects to foster the tissue restoration.^{10–12} However, the possible large surgical wounds, poor implant fit and susceptibility to infection due to incisions accompanying implantation *etc.*, restrained the application of these implanted hydrogels.¹³

As alternative to preformed hydrogels, injectable hydrogels have been paid much attention over the past decade.¹⁴ Typically, the injectable hydrogel is a free flowing solution before administration, and once injected, forms a solid hydrogel by *in situ* chemical crosslinking or by a sol–gel physical phase

transition.^{15–18} Since such hydrogels are formed *in vivo* after injection, they can cause minimal surgical wounds and thus reduce the possibility of infection, while easily fill cavities of arbitrary shapes. However, the possible leakage of liquid precursors to neighboring tissue or the blood stream might also limit their application in some respects, even though fast gelation kinetics and high precursor viscosity can minimize the extent of the leakage.¹⁹

A recent trend in designing injectable hydrogels is focused on the gels with thixotropic properties.^{20–27} These hydrogels are in the solid form before administration, but can shear-thin and subsequently flow under a proper shear stress during injection. After injection, the hydrogels quickly recover into the solid form and are retained as depots at the site of injection. Compared with the single component route,^{20–22} mixing two components to create a preformed injectable hydrogel has received more attention. Various combinations have been employed, including oppositely charged colloidal particles consisting of synthetic poly(D,L-lactic-co-glycolic acid),²³ organic and inorganic composites, *e.g.*, PEG and silica,²⁴ α -cyclodextrin and triblock copolymer containing PEG block,²⁵ and two biomacromolecules, *i.e.*, two polysaccharides or two proteins.^{26,27}

Bombyx mori silkworm cocoon silk, has been used as textile fiber for centuries.²⁸ As a natural protein material, silk fibroin (SF) from *Bombyx mori* silk has been used in many other areas, such as the biomedical, biomineralization and microdevice areas,

^aDepartment of Macromolecular Science, Key Laboratory of Molecular Engineering of Polymers of Ministry of Education, Laboratory of Advanced Materials, Fudan University, 220 Handan Road, Shanghai, 200433, People's Republic of China. E-mail: zzshao@fudan.edu.cn

^bResearch Center for Analysis and Measurement, Fudan University, 220 Handan Road, Shanghai, 200433, People's Republic of China. E-mail: yuhongyang@fudan.edu.cn

† Electronic supplementary information (ESI) available. See DOI: 10.1039/c2sm06984a

etc. in recent decades.^{29–31} SF consists of heavy and light chain polypeptides of *ca.* 390 kDa and *ca.* 25 kDa respectively.³² The SF heavy chain is composed mainly of glycine (G), alanine (A) and serine (S), which constitute the highly repetitive GAGAGS amino acid motif contributing to the formation of a β -sheet structure.²⁸ SF can form hydrogels crosslinked by an intermolecular β -sheet structure.^{33,34} Because of the adjustable mechanical properties and biodegradability related closely to the content of β -sheet crystallinity, SF hydrogels are promising candidates for biomedical applications.²⁹ Although low pH, high temperature, alcohol and shear stress are found to accelerate the gelation process, the gelation time of SF is always a few weeks or months under physiological conditions, which is too long for its application.^{33–37} On the other hand, hydroxypropylcellulose (HPC) is a natural cellulose ether that has been approved for food additives and drug administration by the FDA.³⁸ As a thermosensitive polymer, HPC has lower critical solution temperature (LCST), about 40–45 °C, above which it precipitates rather than gels in water (Fig. 1).

In the present study, we developed a novel blend hydrogel comprising SF and HPC. The blends gelled at 37 °C within 1 h (Fig. 1) and the hydrogel showed thixotropic properties, which is injectable. This blend hydrogel is unique in two ways from previous thixotropic hydrogels: (1) given the fact that the natural extracellular matrix (ECM) is a mixture of proteins and polysaccharides, our blend hydrogel should more closely mimic the function of the ECM and thus be a suitable material for cell delivery; and 2) the polysaccharide, *i.e.*, HPC, has abundant hydroxyl groups, which can be used to modify the polymer for various purposes. According to the analysis of dynamic rheological measurements, confocal laser scanning microscopy (CLSM), Raman and quantitative ¹³C-NMR spectroscopy, we assumed a possible gelation mechanism, while demonstrating that the blend hydrogel could protect encapsulated cells against high shear forces during injection, suggesting that SF–HPC hydrogels may be applied as carrier materials in cell transplantation therapy.

2. Experimental section

Materials

Hydroxypropyl cellulose (HPC) ($M_w = 100\,000$ reported by the manufacturer, DS = 3.0, MS = 3.9 determined by means of NMR spectroscopy according to Tezuka *et al.*³⁹) (DS: the degree

of substitution, *i.e.*, the average number of substituted hydroxyl groups in the monomer unit; MS: the molar substitution, *i.e.*, the average number of oxyethylene moieties per monomer unit) was purchased from Aldrich. Rhodamine B isothiocyanate (RITC; Sigma), 5-carboxyfluorescein (Sigma), *N,N'*-dicyclohexyl carbodiimide (DCC; GL Biochem (Shanghai) Co., Ltd.) and 4-dimethylamioopyridine (DMAP; Shanghai Medpep Co., Ltd.) were used as received.

Preparation of SF, HPC and SF–HPC blend aqueous solution

The degumming and dissolving process of *Bombyx mori* silk followed established procedures.⁴⁰ The resulting SF solution (4–5 wt%) was concentrated to 10 wt% according to the negative pressure method described in our Chinese Patent (CN 201110000201.8).

HPC solution was prepared by dissolving HPC in deionized water at a concentration of 10 wt%. The SF solution and HPC solution were mixed in different proportions at 25 °C to obtain blends with mixing ratios of 7/3, 5/5 and 3/7, which were named SF–HPC30, SF–HPC50, SF–HPC70.

Rheological measurement

All rheological experiments were performed at 37 ± 0.1 °C in the strain-controlled mode using a Physica MCR 301 rheometer (Anton Paar GmbH, Austria) using a cone-and-plate geometry of 1° incline, 60 mm diameter (CP 60/1). To minimize evaporation, a solvent trap was employed and a low viscosity mineral oil was applied around the sample. Dynamic frequency sweep experiments were performed in the range of 0.1–10 Hz at 5% strain. To study the thixotropic properties of the hydrogel, strain sweep in the range of 0.3–3000% and step strain sweep, 3000% strain for 60 s followed by 1% strain, were run at 1 Hz.

Confocal laser scanning microscopy (CLSM)

CLSM observations were carried out on a Leica TCS SP5II laser scanning microscope (Leica, German) in the fluorescence mode. SF was labelled with rhodamine B isothiocyanate (RITC) according to Nagarkar *et al.*,⁴¹ by adding a small amount of a concentrated RITC solution to the SF solution 24 h before blending with labelled HPC solution. The concentration of RITC in the final blend solution was around 5 ppm.

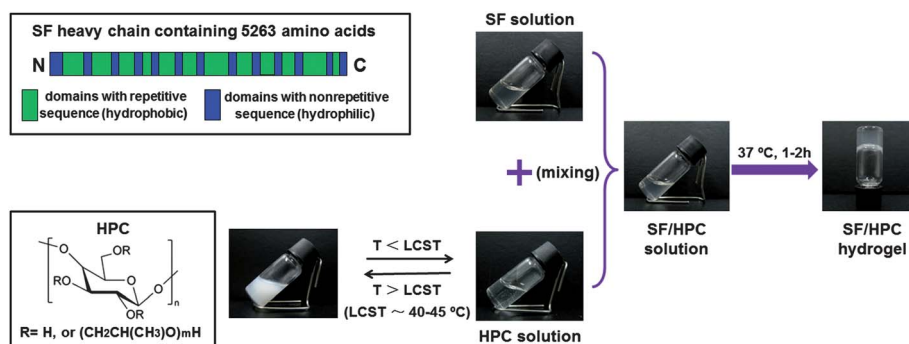


Fig. 1 Schematic representation of SF–HPC hydrogel formation and the structural features of the two biopolymers.

Fluorescein labelled HPC (HPC-Fluo) was synthesized according to the literature procedures with minor modification.⁴² Briefly, 2.0 g of HPC, 0.20 g of DCC and 0.12 g of DMAP were added to a 100 mL three-necked flask. Under protection of nitrogen, 50 mL of dry DMF was then added using a syringe. After all the reagents were dissolved, 15 mg 5-carboxyfluorescein dissolved in 5 mL DMF was added using a syringe. The mixture was stirred first at 0 °C for 1 h and then at room temperature for 24 h. The product was precipitated by addition of ethyl ether. The resulting precipitate was recrystallized from methylene dichloride/ether, and dried under vacuum to obtain the final product.

To prevent syneresis, the blends of labelled SF and HPC were allowed to gel in a sealed space at 37 °C. To minimize the interference between the dyes, the fluorescein (excited at 488 nm) emission filter was set between 500 and 540 nm whereas rhodamine B (excited at 543 nm) emission was recorded between 620 and 660 nm.

Quantitative ¹³C-NMR spectroscopy

Quantitative ¹³C-NMR spectra were acquired with a DMX 500 spectrometer (Bruker, Switzerland) at a carbon frequency of 125 MHz using the inverse gated ¹H decoupling technique. The one-pulse experiments were performed with the 90° pulse length of 6.3 μs. The delay before the application of pulse was 6 s and the acquisition time was 619 ms. The spectral width was 210 ppm with the number of data points 32k. The number of acquired transients was 7000. All the spectra of SF–HPC solutions and hydrogels were acquired at room temperature (25 °C) using the deuterated water as the deuterium ‘lock’ for field stabilization. The hydrogels were *in situ* formed in the sample tube at 37 °C for at least 3 h.

Raman spectroscopy

Raman spectra of SF–HPC blend solutions and hydrogels were recorded with a LabRam-1B Raman microscope (Dilor, France). A He–Ne laser was used to give 6 mW of energy at 632.81 nm. The samples for Raman spectra were frozen rapidly by plunging them into liquid nitrogen and then freeze-dried for two days.

Cell culture and viability assays

L929 mice fibroblast cells were cultured in RPMI 1640 cell culture media supplemented with 10% FBS and 1% penicillin–streptomycin at 37 °C and 5% CO₂. Cells were detached from tissue culture flasks with trypsin, and resuspended in fresh culture media. The cell suspension was added to the SF solution and mixed with HPC solution, resulting in approximately 3 × 10⁵ cells mL⁻¹, 7% SF and 3% HPC. The mixture was incubated at 37 °C for 3 h to allow gelation. The cell encapsulated hydrogel was then loaded into a 1 mL syringe and injected through a 27 gauge needle onto a sample well with a coverslip bottom. The viability of cells was determined using a Live/Dead Viability/Cytotoxicity Kit (Molecular Probes, Invitrogen, Carlsbad, CA). The staining solution containing 2 μM calcein AM and 4 μM EthD-1 was added directly onto the gel and allowed to react for 45 min before observation with CLSM.

3. Results and discussion

Determination of the gel point and the rheological properties of SF–HPC blend hydrogels

The dynamic moduli of SF–HPC30 were measured as a function of frequency at various times during the hydrogel formation process at 37 °C and are shown in Fig. 2. The SF–HPC solution behaved as a viscoelastic fluid (sol) in the first 30 min, where the loss modulus (G'') was higher than storage modulus (G'). Both G' and G'' increased with gel time. After 73 min, G' became larger than G'' , and finally presented nearly frequency-independent behavior in the entire frequency range tested, which was a characteristic of solid (gel)-like behavior.

The frequency independence of loss tangent ($\tan\delta$), which was proposed to be a gel point criterion by Winter and coworkers,⁴³ was investigated to determine the sol–gel transition point in this study. According to the criterion, G' and G'' exhibited power law behavior and the $\tan\delta$ showed frequency independence at the gel point:

$$G'(\omega) \sim G''(\omega) \sim \omega^n \quad (0 < n < 1) \quad (1)$$

$$G''(\omega)/G'(\omega) = \tan\delta = \tan(n\pi/2) \quad (2)$$

$$G'(\omega) = \frac{G''(\omega)}{\tan(n\pi/2)} = S\Gamma(1-n)\cos(n\pi/2)\omega^n \quad (3)$$

where n is defined as a viscoelastic exponent whose value lies between 0 and 1. S is the so-called gel stiffness or gel strength with dimensions of Pa s ^{n} .

The evolution of $\tan\delta$ of such a sample with time (Fig. 3a) shows that there was no clearly frequency-independent $\tan\delta$ during gelation. Thus, the $\tan\delta$ method should be used within a limited frequency range,^{44–46} *i.e.*, 1–10 Hz in our case. Multi-frequency curves of $\tan\delta$ *versus* time passed through a common point (Fig. 3b), which was defined as the critical gel point. For the SF–HPC30 hydrogels, the gel point was found to be after 48 min at 37 °C. Using eqn (2) and eqn (3), the viscoelastic exponent, n , was determined to be 0.84 and S , the gel stiffness at the gel point, was estimated to be 1.3 × 10⁻² Pa s^{0.84}.

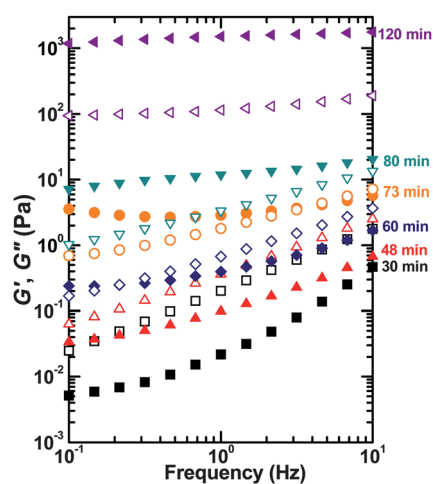


Fig. 2 Storage modulus (G' , filled symbols) and loss modulus (G'' , open symbols) *versus* frequency SF–HPC30 at various time indicated during sol–gel transition at 37 °C.

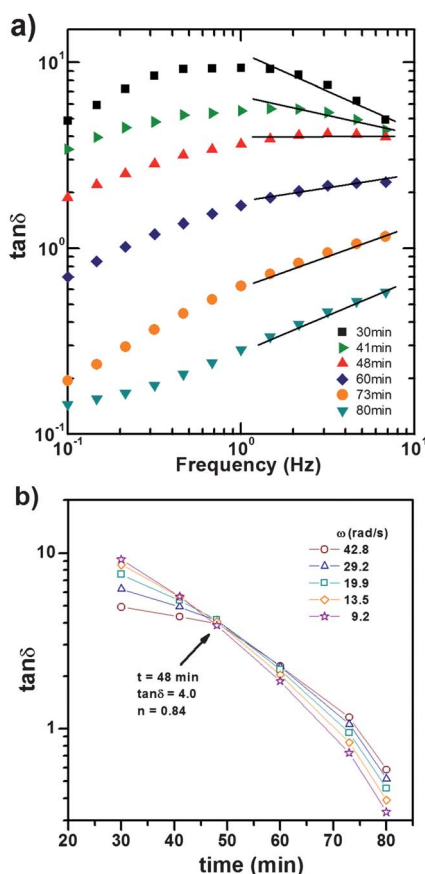


Fig. 3 (a) The loss tangent ($\tan\delta$) versus frequency of SF–HPC30 at various times during the sol–gel transition at 37 °C. (b) $\tan\delta$ as a function of time at various angular frequencies.

For the time just after the gel point, the G' and G'' curves maintained their general shape and exhibited a crossover point at which G' and G'' were equal (e.g. the curves of 60 min and 73 min in Fig. 2). This gave the possibility of building a pair of master curves known as time-cure superposition, which is the superposition of viscoelastic functions for varying extents of gelation. Since the near critical gels are self-similar, a change in the extent of gelation results in a mere change in scale, but the functional form of the viscoelasticity remains the same.⁴⁷ Thus, time-cure superposition enables us, not only to validate the critical gel point determined above, but also to identify the critical scaling exponents of the longest relaxation time and equilibrium modulus, both of which characterize the molecular structure of the gel networks.

By shifting the G' and G'' curves through the characteristic frequency, ω_c and the characteristic modulus, G_c , the master curve for SF–HPC30 are shown in Fig. 4. Here, ω_c is defined as the crossover frequency at which $G' = G''$.^{48,49} The master curve spanning a wide frequency range (over four decades) characterized the viscoelastic relaxation of the SF–HPC hydrogel near the gel point. When the frequency was above ω_c , the clusters trapped within the network governed the viscoelastic behavior, resulting a higher G'' than G' . In contrast, the network was responsible for the viscoelastic behavior which is reflected in typical rheological properties of ideal solid at frequencies below ω_c .⁵⁰

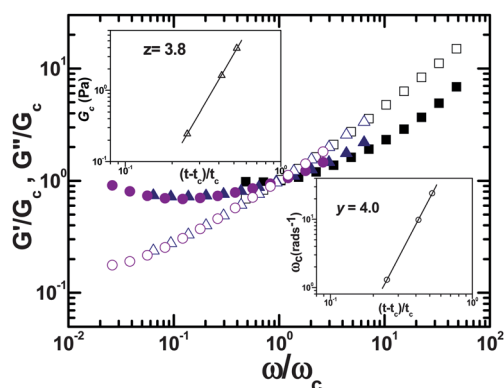


Fig. 4 Collapsed rheological master curve obtained by shifting $G'(\omega)$ (closed symbols) and $G''(\omega)$ (open symbols) through the characteristic (crossover) frequency ω_c and the characteristic (crossover) modulus G_c . Upper inset: G_c versus $(t - t_g)/t_g$, which is the relative distance from the gel point t_g . Lower inset: ω_c versus $(t - t_g)/t_g$.

Near the gel point, the longest relaxation time, τ_L and equilibrium modulus G_e are expected to obey a power law with the relative distance from the gel point, $\varepsilon = (t - t_g)/t_g$:

$$\tau_L \sim \omega_c^{-1} \sim \varepsilon^{-\gamma} \quad (4)$$

$$G_e \sim G_c \sim \varepsilon^z \quad (5)$$

The scaling exponents, γ and z were determined to be 4.0 and 3.8, respectively (insets of Fig. 4).

The gel parameters of SF–HPC hydrogels with different weight ratios are summarized in Table 1. The gelling time (point) gradually decreased with the increase in the proportion of SF in the blends. The values of viscoelastic exponent n lay in the range 0.8–0.9, indicating that all the critical gels were generally very soft and fragile.⁴³ The SF–HPC30 and SF–HPC50 hydrogels had similar values of n , γ and z , which approach the values predicted by Rouse theory ($n = 2/3$, $\gamma = 4$ and $z = 8/3$).^{51,52} On the other hand, the exponents obtained for the SF–HPC70 hydrogel were distinctly different from those of the SF–HPC30 and SF–HPC50 hydrogels, and were in close agreement with the predicted values from Zimm theory ($n = 1$, $\gamma = 8/3$ and $z = 8/3$).^{51,52}

Microstructure of SF–HPC blend hydrogels

Confocal microscopy was employed to gain insight into the gel formation mechanism of SF and HPC blends. Besides the three-dimensional structure, the distribution of these two biopolymers within the hydrogels can be investigated at the same time, as SF was labeled with rhodamine B (red) and HPC was labeled using fluorescein (green).

Fig. 5 shows the confocal microscopy images of SF–HPC30, SF–HPC50 and SF–HPC70. All three hydrogels displayed a drop-matrix structure, that is, spherical droplets, with broad size distributions, rich in one component dispersed in a continuous phase rich in another component. It could be found that HPC dominated the dispersed droplets in the SF–HPC30 hydrogel, whereas the droplets in the SF–HPC50 and SF–HPC70 hydrogels were rich in SF. Compared with the droplets in the SF–HPC50 hydrogel which were up to 150 μm in diameter, the

Table 1 Gel parameters of SF–HPC hydrogels formed at 37 °C

Hydrogel	C_{total} (wt%)	Mix ratio (SF/HPC)	Gel point (min)	n	S (Pa s ^{<i>n</i>})	y	z
SF–HPC30	10	3/7	120	0.90	9.8×10^{-2}	2.5	2.8
SF–HPC50	10	5/5	90	0.79	1.8×10^{-1}	4.3	4.1
SF–HPC70	10	7/3	48	0.84	1.3×10^{-2}	4.0	3.8

droplets in the SF–HPC30 and SF–HPC70 hydrogels were much smaller (below 50 μm). In addition, some droplets in the SF–HPC50 and SF–HPC70 hydrogels appeared to be partially coalescent (Fig. 5e, 5h).

The morphology of the droplet-matrix structure indicated that the gelation of SF–HPC was likely induced by a phase-separation process *via* a nucleation and growth mechanism,^{53,54} which may be triggered by the enhanced intermolecular hydrophobic interaction between HPC chains upon heating to 37 °C. As phase separation proceeded, the dispersed morphology coarsened by either coalescence processes or by Ostwald ripening, *i.e.* the gradual dissolution of the smaller droplets into the larger ones.⁵³ The interaction between the dispersed phase promoted not only the coarsening process, but the gel formation as well, and the space-spanned gel network eventually terminated the coarsening

process. The kinetics of phase separation and gelation could be tuned by changing the composition of the blend, and thus varied the morphology of gel. Due to the trapped phase separation at the initial stage, fewer droplets formed in the SF–HPC30 gel with the fastest gelation kinetics (as shown in Table 1). However, in the SF–HPC50 and SF–HPC70 gels, more droplets and discernible coalescence accompanied by slower gelation kinetics were observed, indicating more extensive coarsening of the phase structure before gel formation.

Molecular mobility in the SF–HPC blend during sol–gel transition

To further understand the gelation mechanism, quantitative ¹³C NMR measurements were performed as they provided the

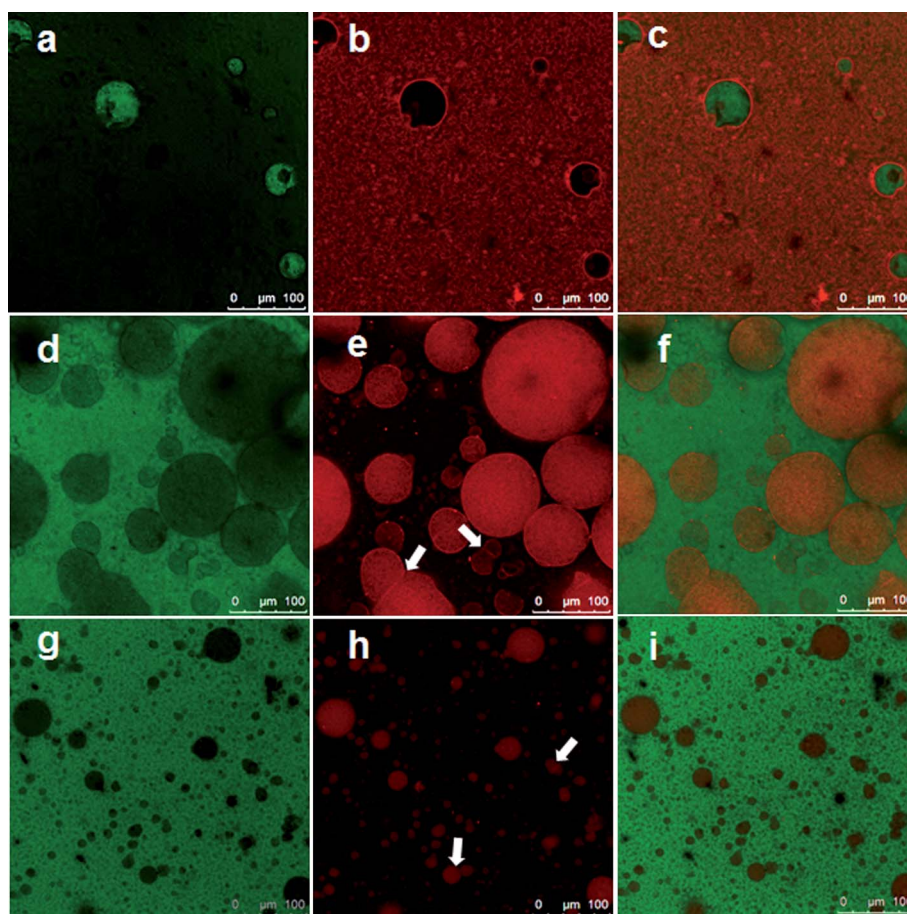


Fig. 5 Confocal laser scanning microscopy (CLSM) images of the SF–HPC hydrogels. (a–c) SF–HPC30, (d–f) SF–HPC50 and (g–i) SF–HPC70. Fluorescein-labeled HPC emit green light (a), (d) and (g) while rhodamine B-labeled SF emit red light (b), (e) and (h). The images (c), (f) and (i) are the overlap of the two corresponding images. The arrows in (e) and (h) indicate partially coalescent droplets.

possibility to investigate the molecular chain mobility of SF and HPC (Fig. 6 and Fig. S1†). For the SF–HPC30 blend, the integral of HPC resonance signals were significantly reduced in the gel state compared with those in solution state. However, the signal intensities of SF remained almost unchanged in both the gel and solution states.

To quantify the differences in the intensity change of individual resonances during the sol–gel transition, we calculated the integral area ratio of HPC at 66–67 ppm, corresponding to the CH carbon at the end of hydroxypropyl substituent,⁵⁵ and that of SF at 50 ppm, corresponding to the C $_{\alpha}$ carbon of Ala residue.⁵⁶ The ratio decreased from 0.91 to 0.20 in the sol–gel transition of the SF–HPC30 blend (Fig. 7), indicating a tremendous decrease in the mobility of HPC molecular chains. It correlated well with the distribution of HPC in the dispersed droplets in the gel state (Fig. 5a–c) and suggested that the mobility of HPC molecular chains was restricted in the phase-separated droplets during the gelation process.

A remarkable increasing in the ratio was observed during the gelation of the SF–HPC70 blend (Fig. 7), which suggested the decrease of the mobility of SF molecular chains. It was also consistent with the phase structure revealed by CLSM (Fig. 5g–i). However, the integral ratios were similar in the solution and the hydrogel of the SF–HPC50 blend (Fig. 7). We suppose that molecular chains of the components in larger

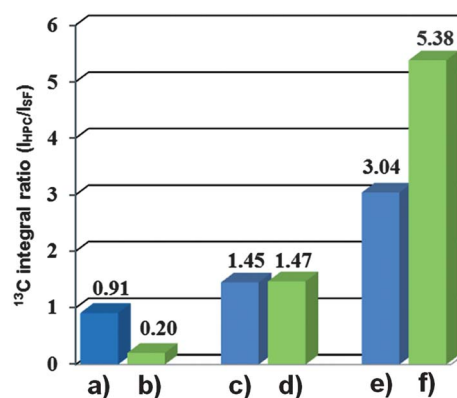


Fig. 7 ¹³C peak integral ratios between HPC and SF (peaks highlighted in Fig. 6) are shown for samples of a) solution, b) hydrogel, SF–HPC30; c) solution, d) hydrogel, SF–HPC50; e) solution, f) hydrogel, SF–HPC70.

dispersed droplets might be less restricted, since the droplets in the SF–HPC50 blend were much larger than other two blends, *i.e.* SF–HPC70 and SF–HPC30 (Fig. 5).

Secondary structural change of SF in the SF–HPC blends during the sol–gel transition

Raman spectra taken close to the gel point of SF–HPC blends were collected to characterize the conformational transition of SF during gelation. According to the literature, the amide I bands around 1659 and 1667 cm⁻¹ are associated with random coil and β-sheet conformations of SF, respectively.^{57,58} The SF–HPC blend solution at 4 °C (to prevent gelation) showed a broad and asymmetric peak at 1659 cm⁻¹ (Fig. 8, curve a), indicating a predominantly random coil conformation along with a small amount of other secondary structures of SF. Upon heating to 37 °C, the broadened peak and the presence of a minor peak near 1681 cm⁻¹ which was assigned to an intermediate conformation between random coil and β-sheet,⁵⁹ indicated that the conformation of SF began to convert from random coil to β-sheet in the initial stage of gelation (Fig. 8, curve b). As the gelation proceeds, it could be found that the β-sheet dominated the secondary structure at the critical gel point (Fig. 8, curve c), suggesting the increase of β-sheet content closely correlating with the gel network formation. As incubation time extended to 120 min (Fig. 8, curve d), the presence of the sharper peak around 1667 cm⁻¹ illustrated a more orderly arrangement of molecular chains as well as the further increase in β-sheet structure of SF. In addition, few other secondary structures were found in the mature of hydrogel, which demonstrated that the β-sheet structure played a role in the crosslinking of the SF–HPC gel network. It is easy to understand that the more content of β-sheets structure in the blend hydrogel, the higher density of the crosslinks can be achieved.

Formation mechanism of SF–HPC blend hydrogels

Based on the discussion above, we proposed a possible hydrogelation mechanism of the SF–HPC blends. As shown in Fig. 9, when the SF–HPC blend solution was heated to 37 °C, the enhancement of intermolecular hydrophobic interactions between HPC molecular chains triggered the phase separation of

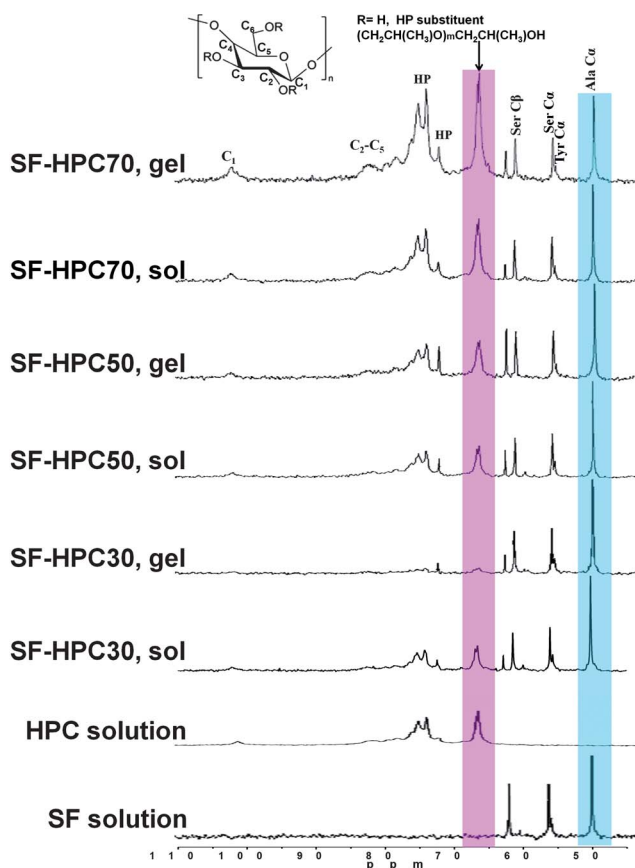


Fig. 6 Quantitative ¹³C NMR spectra of 10 wt% SF–HPC solution and hydrogel with different SF–HPC mix ratios. The peaks of the CH carbon of the end hydroxypropyl substituent (66–67 ppm) and the C $_{\alpha}$ carbon of the Ala residue (50 ppm) are highlighted.

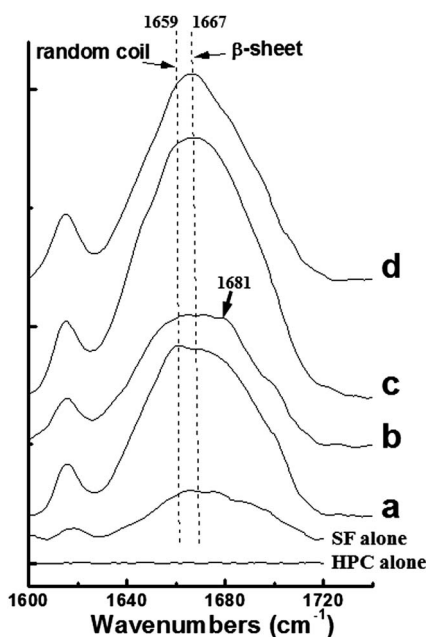


Fig. 8 Amide I region of Raman spectra of SF-HPC30: (a) solution at 4 °C, (b) solution at 37 °C (after 0 min of incubation at 37 °C), (c) near critical gel (after 50 min of incubation at 37 °C) and (d) complete hydrogel (after 120 min of incubation at 37 °C). Raman spectra of 10 wt% SF and HPC solution are also shown as controls.

the blend *via* nucleation and growth mechanism, and finally led to the formation of SF-rich domains. Correspondingly, the local increase in SF concentration was likely to drive the conformational transition of SF from random coil to β -sheet, which resembled the macromolecular crowding effect on protein folding.^{60,61} As phase separation proceeds, the dispersed droplets coarsen, along with the increase of intermolecular β -sheet content till the hydrogel network forms. The significant increase in the β -sheet content at the gel point compared to the sol state indicated that β -sheets may act as crosslinks of the gel network. The further increase in the β -sheet content beyond the gel point resulted in a higher crosslink density and a larger modulus of the hydrogel. This also explained why the gelling time was inversely proportional with the concentration of SF (Table 1). Moreover, since the β -sheet structure is not easy to break, the SF-HPC hydrogel was thermo-irreversible. Besides, the hydrophobic interaction and entanglement between molecular chains may also contribute to the formation of hydrogel network. With the

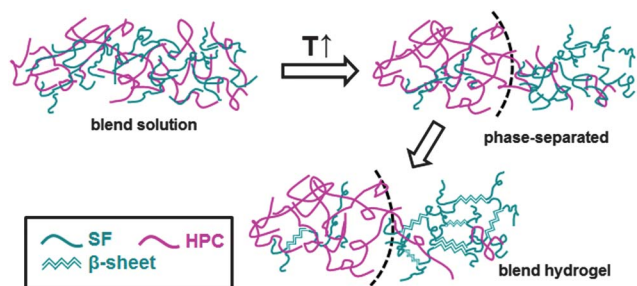


Fig. 9 Schematic illustration of the mechanism of SF-HPC blend hydrogel formation.

improvement of network, the coarsening of the dispersed droplets was arrested by the mature gel network, so the mobility of molecular chains in the dispersed droplets was severely restricted, which eventually gave rise to the “freezing” of the formed phase structure.

Thixotropic properties of the hydrogel and viability of injected cells in the hydrogel

For future application purposes (*e.g.*, delivery of cells), a material that gelled between 10 and 60 min at the physiological temperature was thought to be suitable in terms of handling *in vitro*, providing sufficient time for cell loading on one hand and ensuring gel formation is not too slow to cause cellular sedimentation on the other hand.⁶² Thus, the SF-HPC30 hydrogel with the gel point of 48 min (Table 1) was chosen to test its injectability and its ability to act as a cell delivery vehicle.

Large amplitude oscillatory rheology confirmed the reversible gel-sol-gel property of the SF-HPC30 hydrogel (Fig. 10). In phase I, a strain sweep of 0.3–3000%, was performed on the SF-HPC30 hydrogel. In the gel state, G' was larger than G'' . Above the critical strain (about 30%), G' decreased rapidly, indicating a collapse of the gel to produce a quasi-liquid. In phase II, 3000% strain was applied for 60 s to further liquefy the gel, and then the strain amplitude jumped to 1% to monitor the gel recovery. After the switch of shear strain from 3000% to 1%, the blend immediately exhibited gel behavior with G' significantly higher than G'' and recovered to around 80% of its initial elastic modulus within 5 min. Since the β -sheet structure of SF was not easy to break under the shear force, when the hydrogel fractured into domains and was flowable during shearing, these domains were still crosslinked through the β -sheet structure of SF, thus they could pack together and reform a complete network once shearing ceased. The mechanism of the thixotropic behavior of SF-HPC blend hydrogels will be discussed in detail in the follow-up work.

To evaluate the ability of our SF-HPC blend hydrogel to protect cells during injection, L929 fibroblast cells were encapsulated in the SF-HPC30 hydrogel *ex vivo* and then injected onto

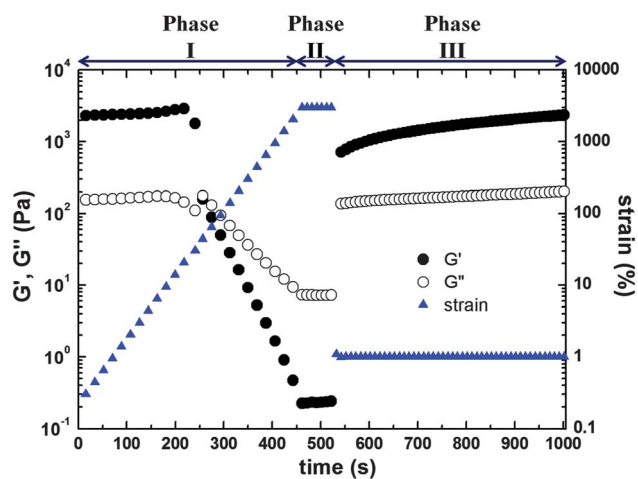


Fig. 10 G' and G'' of a SF-HPC30 hydrogel (incubated at 37 °C for 3 h) on strain sweep (0.3–3000%) and subsequent step strain (3000% and 1%) measurements.

a well for confocal observation *via* a 27-gauge needle. After injection, a live–dead assay was performed on the syringe-delivered cells by staining the live cells green with calcein AM and dead cells red with ethidium homodimer. The vast majority of the L929 cells, over 95%, remained alive after injection (Fig. S2†) and was not significantly different from that observed in the uninjected gels (Fig. S3a†). The negative control with cells killed by methanol showed that the staining conditions are sufficient to identify dead cells (Fig. S3b†). The 3D confocal image also suggested that the cells were still evenly distributed within the injected hydrogel (Fig. 11). Therefore, our hydrogels not only encapsulated cells creating a homogeneous cell/gel construct, regardless of delivery by syringe injection, but also enabled them to survive under high shear stress during injection.

Conclusions

In this work, a novel blend hydrogel comprising SF and HPC was developed. The blends gelled at 37 °C within 1 h and the hydrogels were injectable as they showed thixotropic properties. Based on the results from dynamic rheological measurements, confocal laser scanning microscopy (CLSM), Raman, and quantitative ¹³C-NMR spectroscopy, a possible gelation mechanism was proposed. When the SF–HPC blend solution was heated to 37 °C, the hydrophobic interaction between HPC chains was enhanced and triggered the phase separation of the blend, which induced the emergence of a SF-rich phase, and thus initiated the conformation transition of SF from random coil to β -sheet. As the phase separation preceded, the phase-separated microstructure coarsened. Meanwhile, the β -sheet content of SF increased, and ultimately, a percolated network formed. The β -sheet content of SF increased continuously after the gel point, leading to the ripening of the gel network and the immobilization of the dispersed phase and the molecular chains therein. It was found that the composition of the blend greatly affected on the kinetics of both phase separation and the gelation process, as well as the final morphology and mechanical properties of the hydrogel. Moreover, the hydrogel was demonstrated to encapsulate cells and to protect the encapsulated cells against high shear force during injection. Thus, the injectable SF–HPC blend hydrogel as a minimally invasive formulation may find applications in numerous biomedical fields, such as cell therapy and drug delivery.

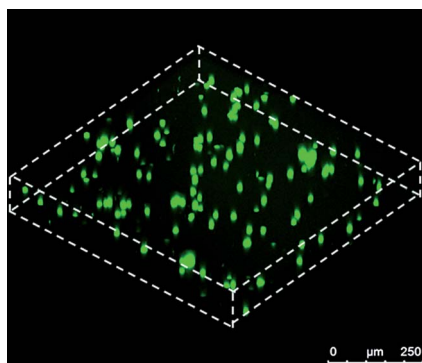


Fig. 11 3D reconstructed CLSM image demonstrating cell survival and homogeneous distribution after injection in the SF–HPC hydrogel.

Acknowledgements

This work was supported by the Natural Science Foundation of China (NSFC 20874018 and 21034003), the 973 Project of Chinese Ministry of Science and Technology (No. 2009CB930000) and State Key Laboratory for Modification of Chemical Fibers and Polymer Materials, DongHua University.

References

- 1 A. M. J. Shapiro, J. R. T. Lakey, E. A. Ryan, G. S. Korbitt, E. Toth, G. L. Warnock, N. M. Kneteman and R. V. Rajotte, *N. Engl. J. Med.*, 2000, **343**, 230–238.
- 2 S. Rafii and D. Lyden, *Nat. Med.*, 2003, **9**, 702–712.
- 3 S. M. Willerth and S. E. Sakiyama-Elbert, *Adv. Drug Delivery Rev.*, 2008, **60**, 263–276.
- 4 S. Kelly, T. M. Bliss, A. K. Shah, G. H. Sun, M. Ma, W. C. Foo, J. Masel, M. A. Yenari, I. L. Weissman, N. Uchida, T. Palmer and G. K. Steinberg, *Proc. Natl. Acad. Sci. U. S. A.*, 2004, **101**, 11839–11844.
- 5 T. M. Bliss, S. Kelly, A. K. Shah, W. C. Foo, P. Kohli, C. Stokes, G. H. Sun, M. Ma, J. Masel, S. R. Kleppner, T. Schallert, T. Palmer and G. K. Steinberg, *J. Neurosci. Res.*, 2006, **83**, 1004–1014.
- 6 A. S. Hoffman, *Adv. Drug Delivery Rev.*, 2002, **54**, 3–12.
- 7 N. A. Peppas, J. Z. Hilt, A. Khademhosseini and R. Langer, *Adv. Mater.*, 2006, **18**, 1345–1360.
- 8 B. V. Slaughter, S. S. Khurshid, O. Z. Fisher, A. Khademhosseini and N. A. Peppas, *Adv. Mater.*, 2009, **21**, 3307–3329.
- 9 C. M. Wang, R. R. Varshney and D. A. Wang, *Adv. Drug Delivery Rev.*, 2010, **62**, 699–710.
- 10 S. J. Bryant, K. L. Durand and K. S. Anseth, *J. Biomed. Mater. Res.*, 2003, **67A**, 1430–1436.
- 11 T. A. Holland, E. W. H. Bodde, L. S. Baggett, Y. Tabata, A. G. Mikos and J. A. Jansen, *J. Biomed. Mater. Res., Part A*, 2005, **75A**, 156–167.
- 12 N. Kodama, M. Nagata, Y. Tabata, M. Ozeki, T. Ninomiya and R. Takagi, *Bone*, 2009, **44**, 699–707.
- 13 R. V. Rughani, M. C. Branco, D. Pochan and J. P. Schneider, *Macromolecules*, 2010, **43**, 7924–7930.
- 14 L. Yu and J. D. Ding, *Chem. Soc. Rev.*, 2008, **37**, 1473–1481.
- 15 Q. Li, J. Wang, S. Shahani, D. D. N. Sun, B. Sharma, J. H. Elisseeff and K. W. Leong, *Biomaterials*, 2006, **27**, 1027–1034.
- 16 M. P. Lutolf, G. P. Raeber, A. H. Zisch, N. Tirelli and J. A. Hubbell, *Adv. Mater.*, 2003, **15**, 888–892.
- 17 M. K. Joo, M. H. Park, B. G. Choi and B. Jeong, *J. Mater. Chem.*, 2009, **19**, 5891–5905.
- 18 J. P. Schneider, D. J. Pochan, B. Ozbas, K. Rajagopal, L. Pakstis and J. Kretsinger, *J. Am. Chem. Soc.*, 2002, **124**, 15030–15037.
- 19 R. N. Shah, N. A. Shah, M. M. D. Lim, C. Hsieh, G. Nuber and S. I. Stupp, *Proc. Natl. Acad. Sci. U. S. A.*, 2010, **107**, 3293–3298.
- 20 L. Haines-Butterick, K. Rajagopal, M. Branco, D. Salick, R. Rughani, M. Pilarz, M. S. Lamm, D. J. Pochan and J. P. Schneider, *Proc. Natl. Acad. Sci. U. S. A.*, 2007, **104**, 7791–7796.
- 21 C. Q. Yan, A. Altunbas, T. Yucel, R. P. Nagarkar, J. P. Schneider and D. J. Pochan, *Soft Matter*, 2010, **6**, 5143–5156.
- 22 B. D. Olsen, J. A. Kornfield and D. A. Tirrell, *Macromolecules*, 2010, **43**, 9094–9099.
- 23 Q. Wang, L. M. Wang, M. S. Detamore and C. Berkland, *Adv. Mater.*, 2008, **20**, 236–239.
- 24 Y. S. Pek, A. C. A. Wan, A. Shekaran, L. Zhuo and J. Y. Ying, *Nat. Nanotechnol.*, 2008, **3**, 671–675.
- 25 J. Li, X. Li, X. P. Ni, X. Wang, H. Z. Li and K. W. Leong, *Biomaterials*, 2006, **27**, 4132–4140.
- 26 D. Gupta, C. H. Tator and M. S. Shoichet, *Biomaterials*, 2006, **27**, 2370–2379.
- 27 C. Foo, J. S. Lee, W. Mulyasmita, A. Parisi-Amon and S. C. Heilshorn, *Proc. Natl. Acad. Sci. U. S. A.*, 2009, **106**, 22067–22072.
- 28 D. Kaplan, W. W. Adams, B. Farmer and C. Viney, *Silk Polymers: Materials Science and Biotechnology*, ACS Symposium Series 544, American Chemical Society, Washington, DC, 1994, pp. 2–16.
- 29 C. Vepari and D. L. Kaplan, *Prog. Polym. Sci.*, 2007, **32**, 991–1007.

- 30 C. Cheng, Z. Z. Shao and F. Vollrath, *Adv. Funct. Mater.*, 2008, **18**, 2172–2179.
- 31 F. G. Omenetto and D. L. Kaplan, *Nat. Photonics*, 2008, **2**, 641–643.
- 32 C. Z. Zhou, F. Confalonieri, M. Jacquet, R. Perasso, Z. G. Li and J. Janin, *Proteins: Struct., Funct., Genet.*, 2001, **44**, 119–122.
- 33 U. J. Kim, J. Y. Park, C. M. Li, H. J. Jin, R. Valluzzi and D. L. Kaplan, *Biomacromolecules*, 2004, **5**, 786–792.
- 34 A. Matsumoto, J. Chen, A. L. Collette, U. J. Kim, G. H. Altman, P. Cebe and D. L. Kaplan, *J. Phys. Chem. B*, 2006, **110**, 21630–21638.
- 35 Z. G. Gong, Y. H. Yang, L. Huang, X. Chen and Z. Z. Shao, *Soft Matter*, 2010, **6**, 1217–1223.
- 36 X. Q. Wang, J. A. Kluge, G. G. Leisk and D. L. Kaplan, *Biomaterials*, 2008, **29**, 1054–1064.
- 37 T. Yucel, P. Cebe and D. L. Kaplan, *Biophys. J.*, 2009, **97**, 2044–2050.
- 38 D. C. Harsh and S. H. Gehrke, *J. Controlled Release*, 1991, **17**, 175–185.
- 39 Y. Tezuka, K. Imai, M. Oshima and T. Chiba, *Carbohydr. Res.*, 1990, **196**, 1–10.
- 40 Y. H. Yang, Z. Z. Shao, X. Chen and P. Zhou, *Biomacromolecules*, 2004, **5**, 773–779.
- 41 S. Nagarkar, T. Nicolai, C. Chassenieux and A. Lele, *Phys. Chem. Chem. Phys.*, 2010, **12**, 3834–3844.
- 42 A. Srivastava, J. H. Waite, G. D. Stucky and A. Mikhailovsky, *Macromolecules*, 2009, **42**, 2168–2176.
- 43 H. H. Winter and M. Mours, *Adv. Polym. Sci.*, 1997, **134**, 165–234.
- 44 D. J. Power, A. B. Rodd, L. Paterson and D. V. Boger, *J. Rheol.*, 1998, **42**, 1021–1037.
- 45 J. H. Choi, S. W. Ko, B. C. Kim, J. Blackwell and W. S. Lyoo, *Macromolecules*, 2001, **34**, 2964–2972.
- 46 R. H. Horst and H. H. Winter, *Macromolecules*, 2000, **33**, 130–136.
- 47 D. Adolf and J. E. Martin, *Macromolecules*, 1990, **23**, 3700–3704.
- 48 X. L. Wang, P. C. Sun, G. Xue and H. H. Winter, *Macromolecules*, 2010, **43**, 1901–1906.
- 49 D. T. N. Chen, K. Chen, L. A. Hough, M. F. Islam and A. G. Yodh, *Macromolecules*, 2010, **43**, 2048–2053.
- 50 P. Tordjeman, C. Fargette and P. H. Mutin, *J. Rheol.*, 2001, **45**, 995–1006.
- 51 J. E. Martin, D. Adolf and J. P. Wilcoxon, *Phys. Rev. Lett.*, 1988, **61**, 2620–2623.
- 52 J. E. Martin and D. Adolf, *Annu. Rev. Phys. Chem.*, 1991, **42**, 311–339.
- 53 M. F. Butler and M. Heppenstall-Butler, *Food Hydrocolloids*, 2003, **17**, 815–830.
- 54 N. Loren and A. M. Hermansson, *Int. J. Biol. Macromol.*, 2000, **27**, 249–262.
- 55 R. N. Ibbett, K. Philp and D. M. Price, *Polymer*, 1992, **33**, 4087–4094.
- 56 T. Asakura, Y. Watanabe, A. Uchida and H. Minagawa, *Macromolecules*, 1984, **17**, 1075–1081.
- 57 P. Monti, G. Freddi, A. Bertoluzza, N. Kasai and M. Tsukada, *J. Raman Spectrosc.*, 1998, **29**, 297–304.
- 58 P. Monti, P. Taddei, G. Freddi, T. Asakura and M. Tsukada, *J. Raman Spectrosc.*, 2001, **32**, 103–107.
- 59 L. Zhou, X. Chen, Z. Z. Shao, Y. F. Huang and D. P. Knight, *J. Phys. Chem. B*, 2005, **109**, 16937–16945.
- 60 A. H. Elcock, *Curr. Opin. Struct. Biol.*, 2010, **20**, 196–206.
- 61 X. J. Ai, Z. Zhou, Y. W. Bai and W. Y. Choy, *J. Am. Chem. Soc.*, 2006, **128**, 3916–3917.
- 62 B. G. Ballios, M. J. Cooke, D. van der Kooy and M. S. Shoichet, *Biomaterials*, 2010, **31**, 2555–2564.